On Attitude Observers and Inertial Navigation for Reference System Fault Detection and Isolation in Dynamic Positioning

Robert H. Rogne*, Tor A. Johansen†, Thor I. Fossen‡,
Center for Autonomous Marine Operations and Systems (AMOS)
Department of Engineering Cybernetics
NTNU - Norwegian University of Science and Technology
7491 Trondheim, Norway
Email: *robert.rogne@itk.ntnu.no †tor.arne.johansen@itk.ntnu.no ‡thor.fossen@itk.ntnu.no

***Abstract*— Marine craft employing a dynamic positioning system rely on measurements from position reference systems and gyrocompasses, and faults in these systems and sensors pose a serious risk of vessel drive-offs, that may in turn have dire consequences. An inertial measurement unit may provide independent position and orientation information, provided that the attitude estimates of the observer in use are accurate enough. In this paper we compare three nonlinear strapdown inertial-measurement-unit-based attitude estimators aided by global navigation satellite systems, and put them to test in a simulation of two fault detection and isolation scenarios. The comparison finds that all attitude estimators under test have the potential for use in a fault detection and isolation scheme.**

I. Introduction

In ship dynamic positioning (DP) Classes 2 and 3, requirements dictate that the vessel must possess three independent position reference (posref) systems and have triple redundancy in vessel sensors ([1],[2],[3]). At the open seas, the common posref systems include taut wire, hydro-acoustic systems and global navigation satellite systems (GNSS), such as GPS, GLONASS and Galileo. The main vessel sensors are gyrocompasses and vertical reference units. These requirements in redundancy are there to improve safety, but their realization is not without challenges.

Especially for the posref systems, satisfying the independence condition is not always easy. These kinds of systems are often in the need of an external aid or reference. For the examples given above we have clump weights and transponders on the sea bed (taut wire and hydro-acoustic, respectively), or satellites in space for GNSS. When the waters are too deep, or operations carry the vessel away from the seabed equipment, the two former cannot be applied, leaving us only with the GNSS option. Relying on more instances of one type of system only can put the safety promised by the redundancy at risk due to common failure modes. In an incident study [4] cited by [5], *"six incidents are classified as drive-off, while five of these six incidents were initiated due to erroneous position data from DGPSs"*.

Also, in addition to the questionable redundancy, there is the unavoidable question of cost. More equipment means higher cost, and since adding more posref systems of the same type does not automatically enhance performance, the cost can be considered superfluous. To improve redundancy, safety, and perhaps even performance, it is therefore enticing to include another set of sensors not found in the DP class requirements today, namely the inertial measurement unit (IMU). IMUs typically measure linear accelerations and angular velocities.

This work was partly supported by the Norwegian Research Council and Rolls-Royce Marine through the MAROFF program together with the Center of Autonomous Marine Operations and Systems (AMOS) at the Norwegian University of Science and Technology (grants no. 225259 and 223254).

A. Inertial Measurement Units and DP

While IMUs are not in widespead use in the DP industry as of today, the idea of using an IMU in conjunction with a posref system is not new ([6],[7],[8],[9]). However, most of the literature focus their efforts on combining inertial sensors with a single posref system for performance reasons. The notion of utilizing an IMU for improving redundancy has been thought of ([10],[11]), but has had limited impact as of yet. [12] investigates using IMUs for fault detection and isolation in DP, but made some limiting assumptions on gyro bias estimation and relying on externally measured roll and pitch.

The low adoption of IMUs in DP so far could be due to the lack of sensors with justifiable cost vs. performance ratio. Yet, with the advent of low-cost, MEMS-based sensors with ever increasing performance, today's and tomorrow's IMUs may enliven the industry's enthusiasm, providing motivation for further research on the topic.

B. Attitude estimation and IMUs

A good attitude estimate is of great importance when integrating the IMUs acceleration output for use in an observer for position and velocity. To obtain high quality estimates of the attitude, one may employ the angular velocities from the IMU, together with vector measurements in the inertial frame such as acceleration and compasses in a sensor fusion scheme ([13], [8], [14], [15], [16], [17]).

C. Main results

In this paper, three nonlinear state-of-the-art attitude estimators are compared, with the motivation for usage in a fault detection and isolation (FDI) setup. In [17], [16], the

observers make use of magnetometer readings as one of the vector measurements, while we employ a gyrocompass instead. The contribution of this paper is related to:

- Attitude observer characteristics and comparison
- Stability of a cascade comprising the nonlinear observers and a translational motion observer aided by GNSS
- Simulation of two FDI cases with posref system and gyrocompass fault.

D. Organization of the paper

In Section II the system kinematics and the observer dynamics are presented. In Section III simulations are carried out in order to evaluate the capabilities of the observers in a DP scenario with one failing posref system or one failing gyrocompass.

II. Attitude observers

A. The concept for comparison and FDI

The three attitude estimators that will be compared are two variants of the nonlinear estimator of [16], and the observer presented in [17]. One of them, as we shall see below, also provides estimates for position and velocity, but these will only be used internally by the observer to aid the attitude estimation. In order to compare them for FDI in position reference systems, a translational motion observer aided by GNSS from [18, Ch. 11] will be added in cascade to all observers.

Fig. 1 shows the structure employed for detection and isolation of faults in either of the two posref systems, GNSS 1 and 2, or either of the two gyrocompasses. The notation is explained in Section II-B. All the observers in Fig. 1 are identical, only the inputs differ between them. A fault can be easily be detected by comparing the measurements directly, since diverging values will indicate a fault. Isolation of the fault on the other hand will require some form of analysis of the observer outputs, and then tracing the fault back to the sensors feeding the observer.

For the simulation tests in this paper three such setups will be simulated in parallel, in order to compare the observers presented in later sections.

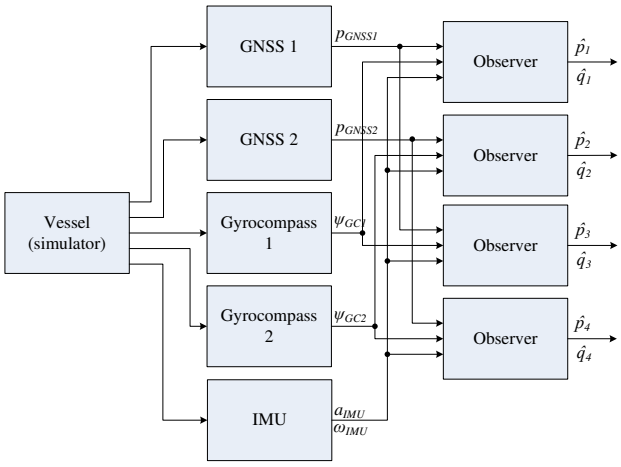

Fig. 1. Four observers in parallel.

B. General assumptions and notation

The following assumptions and simplifications are made:

- Earth rotation is neglected and the North-East-Down frame is assumed to be the inertial reference.
- IMU accelerometer biases are neglected, i.e. biases are assumed to be accounted for in calibration.
- No lever arms between measuring equipment and vessel origin.

The same notation as in [18] is used:

- $\boldsymbol{p}^n_{m/n}$ - position of the point o_m with respect to $\{n\}$ expressed in $\{n\}$
- $\boldsymbol{v}^n_{m/n}$ - linear velocity of the point o_m with respect to $\{n\}$ expressed in $\{n\}$
- ψ - yaw angle between between $\{b\}$ and $\{n\}$
- $\boldsymbol{\omega}^b_{b/n}$ - body-fixed angular velocity
- $\boldsymbol{b}^b$ - gyro bias
- $\boldsymbol{R}^n_b$ and $\boldsymbol{R}^b_n = \boldsymbol{R}^{n\top}_b$ are the rotation matrices to $\{n\}$ from $\{b\}$ and vice versa, respectively
- $\boldsymbol{q}$ - quaternion representation of rotation $\{b\}$ to $\{n\}$
- $\boldsymbol{S}(\boldsymbol{x})$ - skew symmetric matrix:

$$\boldsymbol{S}(\boldsymbol{x}) = \begin{bmatrix} 0 & -x_3 & x_2 \\ x_3 & 0 & -x_1 \\ -x_2 & x_1 & 0 \end{bmatrix}, \ \boldsymbol{x} = \begin{bmatrix} x_1 \\ x_2 \\ x_3 \end{bmatrix}$$

- $\boldsymbol{g}^n$ - local gravity vector in $\{n\}$
- $\boldsymbol{a}^b_{IMU}$ - accelerometer specific force measurement in the body/vessel frame $\{b\}$
- $\boldsymbol{\omega}^b_{IMU}$ - angular velocity measurement of the body
- $\boldsymbol{p}^n_{GNSS}$ - position measurement
- ψ_{GC} - gyrocompass heading measurement

The kinematics of the system can be described as follows:

$$\dot{\boldsymbol{p}}^n_{m/n} = \boldsymbol{v}^n_{m/n} \tag{1a}$$
$$\dot{\boldsymbol{v}}^n_{m/n} = \boldsymbol{R}^n_b(\boldsymbol{q})\boldsymbol{a}^b + \boldsymbol{g}^n \tag{1b}$$
$$\dot{\boldsymbol{q}} = \frac{1}{2}\boldsymbol{\Omega}(\boldsymbol{\omega}^b_{b/n})\boldsymbol{q} \tag{1c}$$
$$\boldsymbol{p}^n_{GNSS} = \boldsymbol{p}^n_{m/n} + \boldsymbol{w}_p \tag{1d}$$
$$\psi_{gc} = \psi + w_\psi \tag{1e}$$

where

$$\boldsymbol{\Omega}(\boldsymbol{x}) = \begin{bmatrix} \boldsymbol{0} & -\boldsymbol{x}^\top \\ \boldsymbol{x} & -\boldsymbol{S}(\boldsymbol{x}) \end{bmatrix} \tag{2}$$

where $\boldsymbol{w_p}$ and w_ψ represent disturbances or measurement faults on the position and heading, respectively. The disturbances will change according to various faults that might occur in the measuring equipment.

C. Nonlinear Observer 1

1) Nonlinear Observer 1a: This observer is a further development of the *Explicit complementary filter with bias correction* described in [14]. Observer equations from [16], sans GNSS velocity measurements and using gyrocompass

heading instead of magnetometer for the second vector measurement:

$$\dot{\hat{\boldsymbol{p}}}^n_{m/n} = \hat{\boldsymbol{v}}^n_{m/n} + \theta \boldsymbol{K}_{pp}(\boldsymbol{p}^n_{GNSS} - \hat{\boldsymbol{p}}^n_{m/n}) \tag{3a}$$

$$\dot{\hat{\boldsymbol{v}}}^n_{m/n} = \hat{\boldsymbol{a}}^n + \boldsymbol{g}^n + \theta^2 \boldsymbol{K}_{vp}(\boldsymbol{p}^n_{GNSS} - \hat{\boldsymbol{p}}^n_{m/n}) \tag{3b}$$

$$\dot{\boldsymbol{\xi}} = -\boldsymbol{R}^n_b(\hat{\boldsymbol{q}})\boldsymbol{S}(\hat{\boldsymbol{\sigma}})\boldsymbol{a}^b_{IMU} + \theta^3 \boldsymbol{K}_{\xi p}(\boldsymbol{p}^n_{GNSS} - \hat{\boldsymbol{p}}^n_{m/n}) \tag{3c}$$

$$\dot{\hat{\boldsymbol{q}}} = \frac{1}{2}\boldsymbol{\Omega}(\hat{\boldsymbol{\omega}})\hat{\boldsymbol{q}} \tag{3d}$$

$$\dot{\hat{\boldsymbol{b}}}^b = \text{Proj}(\hat{\boldsymbol{b}}^b, -k_I\hat{\boldsymbol{\sigma}}) \tag{3e}$$

$$\hat{\boldsymbol{a}}^n = \boldsymbol{R}^n_b(\hat{\boldsymbol{q}})\boldsymbol{a}^b_{IMU} + \boldsymbol{\xi} \tag{3f}$$

$$\hat{\boldsymbol{\sigma}} = k_1 \boldsymbol{v}^b_1 \times \boldsymbol{R}^{n\top}_b(\hat{\boldsymbol{q}})\boldsymbol{v}^n_1 + k_2 \boldsymbol{v}^b_2 \times \boldsymbol{R}^{n\top}_b(\hat{\boldsymbol{q}})\boldsymbol{v}^n_2 \tag{3g}$$

$$\hat{\boldsymbol{\omega}} = \boldsymbol{\omega}^b_{IMU} - \hat{\boldsymbol{b}} + \hat{\boldsymbol{\sigma}} \tag{3h}$$

where $\boldsymbol{K}_{pp}$, $\boldsymbol{K}_{pp}$ and $\boldsymbol{K}_{\xi p}$ are gain matrices chosen such that $\boldsymbol{A} - \boldsymbol{K}\boldsymbol{C}$ is Hurwitz, where

$$A = \begin{bmatrix} \boldsymbol{0} & \boldsymbol{I}_3 & \boldsymbol{0} \\ \boldsymbol{0} & \boldsymbol{0} & \boldsymbol{I}_3 \\ \boldsymbol{0} & \boldsymbol{0} & \boldsymbol{0} \end{bmatrix}, C = \begin{bmatrix} \boldsymbol{I}_3 & \boldsymbol{0} & \boldsymbol{0} \end{bmatrix} K = \begin{bmatrix} \boldsymbol{K}_{pp} \\ \boldsymbol{K}_{vp} \\ \boldsymbol{K}_{\xi p} \end{bmatrix}$$

Furthermore, θ is a tuning parameter larger than or equal to 1, used to guarantee stability, $k_I > 0$ is a gain, $\text{Proj}(\cdot,\cdot)$ is a parameter projection that puts a restriction on the estimate $\hat{\boldsymbol{b}}^b$, see [15] for details. k_1 and k_2 of the injection term $\hat{\boldsymbol{\sigma}}$ are gains satisfying $k_1 \geq k_p$ and $k_2 \geq k_p$ for a $k_p > 0$. The other factors of (3) are:

$$\boldsymbol{v}^b_1 = \frac{\boldsymbol{a}^b_{IMU}}{||\boldsymbol{a}^b_{IMU}||},\ \boldsymbol{v}^b_2 = \frac{\boldsymbol{a}^b_{IMU} \times \boldsymbol{c}^b}{||\boldsymbol{a}^b_{IMU} \times \boldsymbol{c}^b||}$$

$$\boldsymbol{v}^n_1 = \frac{\hat{\boldsymbol{a}}^n}{||\hat{\boldsymbol{a}}^n||},\ \boldsymbol{v}^n_2 = \frac{\hat{\boldsymbol{a}}^n \times \boldsymbol{c}^n}{||\hat{\boldsymbol{a}}^n \times \boldsymbol{c}^n||} \tag{4}$$

where

$$\boldsymbol{c}^b = \begin{bmatrix} \cos(\psi_{gc}) \\ -\sin(\psi_{gc}) \\ 0 \end{bmatrix},\ \boldsymbol{c}^n = \begin{bmatrix} 1 \\ 0 \\ 0 \end{bmatrix} \tag{5}$$

The position and velocity, and attitude estimators of Nonlinear Observer 1 form a feedback interconnection. In [16], this feedback interconnection is proved to have a uniform semi-global exponentially stable (USGES) equilibrium point.

2) Nonlinear Observer 1b: From (3) we notice that p^n_{GNSS} is part of the observer equations of Nonlinear Observer 1. In the case of a GNSS fault, this signal cannot be trusted, and may cause errors in the attitude estimation and FDI. We therefore also test Nonlinear Observer 1a without the feedback interconnection, and call the resulting observer Nonlinear Observer 1b. In this case, the feedback from the position estimate is removed. This is achieved by instead of (4), using:

$$\boldsymbol{v}^b_1 = -\frac{\boldsymbol{a}^b_{IMU}}{||\boldsymbol{g}^n||},\ \boldsymbol{v}^b_2 = -\frac{\boldsymbol{a}^b_{IMU} \times \boldsymbol{c}^b}{||\boldsymbol{g}^n \times \boldsymbol{c}^n||}$$

$$\boldsymbol{v}^n_1 = \frac{\boldsymbol{g}^n}{||\boldsymbol{g}^n||},\ \boldsymbol{v}^n_2 = \frac{\boldsymbol{g}^n \times \boldsymbol{c}^n}{||\boldsymbol{g}^n \times \boldsymbol{c}^n||} \tag{6}$$

where $\boldsymbol{g}^n = [0\ 0\ g]^\top$.

D. Nonlinear Observer 2

This observer is also based on the *Explicit complementary filter with bias correction* described in [14]. Observer equations from [17], using gyrocompass instead of magnetometer for the second vector measurement:

$$\dot{\hat{\boldsymbol{q}}} = \frac{1}{2}\boldsymbol{\Omega}(\hat{\boldsymbol{\omega}})\hat{\boldsymbol{q}} \tag{7a}$$

$$\dot{\hat{\boldsymbol{b}}}^b = -k_b\hat{\boldsymbol{b}}^b + k_b \text{sat}_\Delta(\hat{\boldsymbol{b}}^b) - \boldsymbol{\sigma_b} \tag{7b}$$

$$\boldsymbol{\sigma_R} = k_1 \boldsymbol{v}^b_1 \times \hat{\boldsymbol{v}}^b_1 + k_2 \hat{\boldsymbol{v}}^b_1 \hat{\boldsymbol{v}}^{b\top}_1 (\boldsymbol{v}^b_2 \times \hat{\boldsymbol{v}}^b_2) \tag{7c}$$

$$\boldsymbol{\sigma_b} = k_3 \boldsymbol{v}^b_1 \times \hat{\boldsymbol{v}}^b_1 + k_4 \boldsymbol{v}^b_2 \times \hat{\boldsymbol{v}}^b_2 \tag{7d}$$

$$\hat{\boldsymbol{\omega}} = \boldsymbol{\omega}^b_{IMU} - \hat{\boldsymbol{b}} + \boldsymbol{\sigma_R} \tag{7e}$$

where

$$\boldsymbol{v}^b_1 = -\frac{\boldsymbol{a}^b_{IMU}}{g},\ \boldsymbol{v}^b_2 = \frac{\pi_{\boldsymbol{v}^b_1}\boldsymbol{c}^b}{||\pi_{\boldsymbol{v}^n_1}\boldsymbol{c}^n||}$$

$$\boldsymbol{v}^n_1 = \begin{bmatrix} 0 \\ 0 \\ 1 \end{bmatrix},\ \boldsymbol{v}^n_2 = \frac{\pi_{\boldsymbol{v}^n_1}\boldsymbol{c}^n}{||\pi_{\boldsymbol{v}^n_1}\boldsymbol{c}^n||} \tag{8}$$

$$\hat{\boldsymbol{v}}^b_1 = \boldsymbol{R}^{n\top}_b(\hat{\boldsymbol{q}})\boldsymbol{v}^n_1,\ \hat{\boldsymbol{v}}^b_2 = \boldsymbol{R}^{n\top}_b(\hat{\boldsymbol{q}})\boldsymbol{v}^n_2$$

$$\pi_{\boldsymbol{x}} = ||\boldsymbol{x}||^2\boldsymbol{I}_3 - \boldsymbol{x}\boldsymbol{x}^\top$$

Furthermore, k_1, k_2, k_3, k_4, k_b and Δ are positive numbers. $\text{sat}_\Delta(\cdot)$ denotes the saturation function $\text{sat}_\Delta(\boldsymbol{x}) = \boldsymbol{x}\min(1, \Delta/||\boldsymbol{x}||)$. k_3 must be chosen to be strictly larger than k_4.

In [17], the observer (7) is proven to be "almost-globally stable" and locally exponentially stable, meaning that [17] *"for almost all initial conditions (...) the trajectory* $(\hat{\boldsymbol{R}}(t), \hat{\boldsymbol{b}}(t))$ *converges to the trajectory* $(\boldsymbol{R}(t), \boldsymbol{b}(t))$*"*, where $\hat{\boldsymbol{R}} = \boldsymbol{R}^n_b(\hat{\boldsymbol{q}})$ and $\boldsymbol{R} = \boldsymbol{R}^n_b(\boldsymbol{q})$. In total there are three initial conditions from which the observer will not converge, each one an unstable equilibrium point [17].

E. Translational Motion Observer aided by GNSS

The observer presented is basically the same as one found in [18, Ch. 11] sans accelerometer bias estimation:

$$\dot{\hat{\boldsymbol{p}}}^n_{m/n} = \hat{\boldsymbol{v}}^n_{m/n} + \boldsymbol{K}_1(\boldsymbol{p}^n_{GNSS} - \hat{\boldsymbol{p}}^n_{m/n}) \tag{9a}$$

$$\dot{\hat{\boldsymbol{v}}}^n_{m/n} = \boldsymbol{R}^n_b(\hat{\boldsymbol{q}})\boldsymbol{a}^b_{imu} + \boldsymbol{g}^n + \boldsymbol{K}_2(\boldsymbol{p}^n_{GNSS} - \hat{\boldsymbol{p}}^n_{m/n}) \tag{9b}$$

This observer was also employed with success in [12] together with basic heading estimation, albeit under the assumption of known pitch and roll.

1) Stability of Nonlinear Observer and Translational Motion Observer in cascade: From (1) and (9), we obtain the following error dynamics for the Translational Motion Observer, without disturbances:

$$\dot{\tilde{\boldsymbol{p}}}^n_{m/n} = \tilde{\boldsymbol{v}}^n_{m/n} - \boldsymbol{K}_1\tilde{\boldsymbol{p}}^n_{m/n} \tag{10a}$$

$$\begin{aligned}\dot{\tilde{\boldsymbol{v}}}^n_{m/n} &= (\boldsymbol{R}^n_b(\boldsymbol{q}) - \boldsymbol{R}^n_b(\hat{\boldsymbol{q}}))\boldsymbol{a}^b_{imu} - \boldsymbol{K}_2\tilde{\boldsymbol{p}}^n_{m/n} \\ &= (\boldsymbol{I}_3 - \tilde{\boldsymbol{R}}^{n\top}_b)\boldsymbol{R}^n_b\boldsymbol{a}^b_{imu} - \boldsymbol{K}_2\tilde{\boldsymbol{p}}^n_{m/n}\end{aligned} \tag{10b}$$

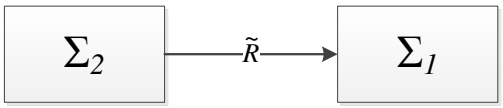

Fig. 2. Cascade connection.

where $\tilde{\boldsymbol{p}}^n_{m/n} = \boldsymbol{p}^n_{m/n} - \hat{\boldsymbol{p}}^n_{m/n}$, $\tilde{\boldsymbol{v}}^n_{m/n} = \boldsymbol{v}^n_{m/n} - \hat{\boldsymbol{v}}^n_{m/n}$ and $\tilde{\boldsymbol{R}}^n_b = \boldsymbol{R}^n_b(\boldsymbol{q})\boldsymbol{R}^n_b(\hat{\boldsymbol{q}})^\top$ is the error rotation matrix .

Proposition 1: Let (10) and the error dynamics of Nonlinear Observer 1 or 2 be connected like in Fig. 2, with (10) as $\boldsymbol{\Sigma}_1$ and the Nonlinear Observer error dynamics as $\boldsymbol{\Sigma}_2$, the tuning parameters $\boldsymbol{K}_1$ and $\boldsymbol{K}_2$ are chosen such that the matrix

$$\boldsymbol{A}_{pv} := \begin{bmatrix} -\boldsymbol{K}_1 & \boldsymbol{I}_3 \\ -\boldsymbol{K}_2 & \boldsymbol{0} \end{bmatrix}$$

is Hurwitz, and the tuning parameters of the Nonlinear Observers satisfy the conditions found in [16] or [17]. If all measured signals and biases are bounded, then the origin of the observer error dynamics for the cascade comprising $\boldsymbol{\Sigma}_1$ and $\boldsymbol{\Sigma}_2$ retains the stability properties of $\boldsymbol{\Sigma}_2$.

Proof: Define the interconnection between $\boldsymbol{\Sigma}_2$ and $\boldsymbol{\Sigma}_1$ as $\boldsymbol{h}(t, \tilde{\boldsymbol{R}}^n_b) := (\boldsymbol{I}_3 - \tilde{\boldsymbol{R}}^{n\top}_b)\boldsymbol{R}^n_b(t)\boldsymbol{a}^b_{imu}(t)$. It can be shown that

$$\begin{aligned} ||\boldsymbol{h}(t, \tilde{\boldsymbol{R}}^n_b)|| &= ||(\boldsymbol{I}_3 - \tilde{\boldsymbol{R}}^{n\top}_b)\boldsymbol{R}^n_b\boldsymbol{a}^b_{imu}|| \\ &= ||(\boldsymbol{I}_3 - \tilde{\boldsymbol{R}}^{n\top}_b)\boldsymbol{a}^b_{imu}|| \\ &\leq 2a_{max}||\tilde{\boldsymbol{\varepsilon}}|| \end{aligned} \tag{11}$$

where $a_{max} = \max(||\boldsymbol{a}^b_{imu}||)$, $\tilde{\boldsymbol{\varepsilon}} = [\tilde{\varepsilon}_1\ \tilde{\varepsilon}_2\ \tilde{\varepsilon}_3]$ is the vector part of the quaternion $\tilde{\boldsymbol{q}}$ associated with $\tilde{\boldsymbol{R}}^n_b$, and $||\tilde{\boldsymbol{\varepsilon}}|| \to 0$ as $\tilde{\boldsymbol{R}}^n_b \to \boldsymbol{I}_3$. Above we have used the properties that $||\boldsymbol{R}^n_b|| = 1$ and $||\boldsymbol{I}_3 - \tilde{\boldsymbol{R}}^{n\top}_b|| = ||\tilde{\eta}\boldsymbol{S}(\tilde{\boldsymbol{\varepsilon}}) - \boldsymbol{S}(\tilde{\boldsymbol{\varepsilon}})^2|| \leq 2||\tilde{\boldsymbol{\varepsilon}}||$ [16], where $\tilde{\eta}$ is the scalar part of $\tilde{\boldsymbol{q}}$. With the condition of (11), and making sure $\boldsymbol{A}_{pv}$ is Hurwitz, we now have a USGES subsystem in the case of Nonlinear Observer 1, or an "almost-globally stable" and locally exponentially stable subsystem in the case of Nonlinear Observer 2, connected to a globally exponentially stable linear system by a linearly bounded interconnection $\boldsymbol{h}(t, \tilde{\boldsymbol{R}}^n_b)$. According to cascade theory ([19]), the cascade then retains the stability properties of $\boldsymbol{\Sigma}_2$. ■

F. Implementation

The nonlinear attitude observers are implemented using the proposed implementation in [17], using exact integration of (3d) and (7a):

$$\hat{\boldsymbol{q}}_{k+1} = \left(\cos\left(\frac{T||\hat{\boldsymbol{\omega}}_k||}{2}\right)\boldsymbol{I}_4 + \frac{T}{2}\text{sinc}\left(\frac{T||\hat{\boldsymbol{\omega}}_k||}{2}\right)\boldsymbol{\Omega}(\hat{\boldsymbol{\omega}}_k)\right)\hat{\boldsymbol{q}}_k$$

where $\text{sinc}(x) = \sin(x)/x$ and T is the time step.

G. Observer comparison

The attitude observers employ many of the same principles, such as fusing vector measurements with IMU gyro output, and putting a bound on the estimate of the gyro bias $\hat{\boldsymbol{b}}^b$ by using the saturation function or the projection algorithm. This is natural as they are all extensions of the work found in [14].

However, there are some major differences, the most important of which are the vectors chosen for $\boldsymbol{v}^b_1$ and $\boldsymbol{v}^n_1$. In Nonlinear Observer 2 ([17]), an assumption is made that $\boldsymbol{a}^b_{IMU} \approx -g\boldsymbol{R}^n_b\boldsymbol{e}_3$, where $\boldsymbol{e}_3 = [0\ 0\ 1]^\top$. This means that $\ddot{\boldsymbol{p}}^n$, i.e. the vehicle's acceleration in the inertial frame n is considered negligible, and that the accelerometer measures mainly the gravity components. This is also the case for Nonlinear Observer 1b. In Nonlinear Observer 1a ([16]) on the other hand, an estimate $\hat{\boldsymbol{a}}^n$ of $\ddot{\boldsymbol{p}}^n$ is made with the help of position measurements, and the estimate is fed into the injection term $\hat{\boldsymbol{\sigma}}$, ideally providing more accurate information. This will become apparent if the vehicle on which the observers are employed is faced with rotational motion or fast translational motion, inducing Coriolis acceleration. Only the former will be an issue in a DP scenario, where the vessel may be exposed to waves causing the vessel to oscillate in all six degrees of freedom.

Another difference between the observers is that Nonlinear Observer 2 provides a global decoupling of the roll and pitch estimations from the yaw estimations. Their motivation is the somewhat untrustworthy properties of the magnetometer used for yaw estimation, and the magnetometer's effect on roll and pitch without this decoupling ([17], [20]). We employ a gyrocompass instead, but still it gives the opportunity to tune the yaw estimation independently of roll and pitch. This could prove valuable for FDI in gyrocompasses.

H. Fault detection and isolation

Various methods for FDI can be found in for instance [21], [22] and [23]. In this paper however, since the main focus is on the comparison of the different nonlinear observers, we will base the FDI scheme on simple threshold values both for detection and identification. We will also limit ourselves to detecting and isolating faults that appear as a semi-slow signal drift, meaning here drifts that are slow enough to be difficult to detect and isolate immediately, but fast enough to put the operation at risk. In our DP scenario, we define this to be position and compass drifts below 1 m/s and 1 deg/s, respectively.

For detection of a fault, we will use the distance between the two measurements we have available. When the distance reaches a certain threshold $thld_{det}$, a fault will be indicated, see Algorithm 1 for a GNSS example. When choosing the threshold value, one must take into account normal sensor drifting, as to avoid false positives.

The next step is isolation. [12] provides a discussion on how sensor faults will affect the equilibrium points of the observer, and how the measurement error of the observer may be used for isolation. For example, if the GNSS is measuring values that differ too much from what the observer is estimating based on the IMU data, the measurement error $\tilde{\boldsymbol{p}} = \boldsymbol{p}_{GNSS} - \hat{\boldsymbol{p}}$ will have a transient response. Here we will monitor the outputs the Translational Motion Observers' position error for the GNSS, and the nonlinear attitude

Algorithm 1 GNSS fault detection by threshold

$x_1 = p_{GNSS1,x}$, $y_1 = p_{GNSS1,y}$
$x_2 = p_{GNSS2,x}$, $y_2 = p_{GNSS2,y}$
$r = \sqrt{(x_1 - x_2)^2 + (y_1 - y_2)^2}$

if $r > thld_{det,GNSS}$ **then**
    Fault detected.

Algorithm 2 GNSS fault isolation by threshold

for i = 1, i<=4, i++ **do**
    $j =$ GNSS connected to observer i
    $\tilde{p}_{i,x} = p_{GNSSj,x} - \hat{p}_{i,x}$, $\tilde{p}_{i,y} = p_{GNSSj,y} - \hat{p}_{i,y}$
    $r_i = \sqrt{\tilde{p}_{i,x}^2 + \tilde{p}_{i,y}^2}$

    if $r_i > thld_{iso,GNSS}$ **then**
        Fault in GNSS j.

observers' yaw (or heading) error for the gyrocompasses, and check if the error passes a given threshold $thld_{iso}$, see Algorithm 2. The observers in the algorithm correspond to the ones in Fig. 1.

I. Observer tuning

The main objective of the observers is the detection and isolation of faults, so gains should be chosen with that in mind, while at the same time addressing the effects of noise and other error sources. One should choose to have a not-so-aggressive feedback, to keep the transients lingering for a while, such that the feedback does not hide the fault. On the other hand, setting the gains too low could hamper the estimating qualities of the observer too much, introducing lag and possibly lowering the performance to the point where one would not be able to isolate faults at all.

With basis in the gains and parameters for the observers found in their respective papers ([16], [17], [12]), we performed a tuning process by trial and error. Nonlinear Observer 1a turned out to be somewhat more difficult to tune than the other observers. This is due to the feedback interconnection structure of the former, meaning that tuning the position estimation part is affecting the attitude estimation, and vice versa. In Nonlinear Observer 2, we also have a separation of yaw from roll and pitch, simplifying the tuning process since the gains can be tuned somewhat independently. After the tuning process, we opted for the following tuning parameters:

1) Nonlinear Observer 1a:

$$k_1 = 0.5,\ k_2 = 0.5,\ k_I = 0.03$$
$$\theta = 3,\ \boldsymbol{K}_{pp} = 0.6\boldsymbol{I}_3,\ \boldsymbol{K}_{vp} = 0.11\boldsymbol{I}_3,\ \boldsymbol{K}_{\xi p} = 0.006\boldsymbol{I}_3$$

and a parameter projection ensuring $||\hat{\boldsymbol{b}}^b|| \leq 0.51$ deg/s.

2) Nonlinear Observer 1b:

$$k_1 = 0.1,\ k_2 = 0.5,\ k_I = 0.03$$

and a parameter projection ensuring $||\hat{\boldsymbol{b}}^b|| \leq 0.51$ deg/s.

3) Nonlinear Observer 2:

$$k_1 = 0.1,\ k_2 = 0.5,\ k_3 = 0.006,\ k_4 = 0.005$$
$$k_b = 8,\ \Delta = 0.03$$

4) Translational motion observer:

$$\boldsymbol{K}_1 = 0.1\boldsymbol{I}_3,\ \boldsymbol{K}_2 = 0.001\boldsymbol{I}_3$$

III. Simulation

The simulations were carried out in MATLAB/Simulink R2013b using a dynamic ship simulator in full 6-DOF, with waves, vibration and measurement noise [24]. All measurements were set to have a zero mean normally distributed noise, except for the posref systems that have a Gauss-Markov process, see Table I for their parameters. The IMU had a sampling frequency of 100 Hz, the GNSS 5 Hz, and the gyrocompass 10 Hz. The observers in this paper was not part of the feedback loop for the simulated DP system, as it is only employed for fault detection and isolation.

A. Case 1: Attitude estimation test

In the first case, a simulation of fault free operation was carried out. No faults were simulated, as the goal of this test was to compare the performance of the estimators.

As we can see from Fig. 3 - 8, all attitude observers manage well, but Nonlinear Observer 1a seems to have the edge when it comes to bias, roll and pitch estimation. For Nonlinear Observer 1b and 2 in Fig. 7 some of the wave motion seems to pollute the bias estimates on roll and pitch, relating to one of the key points of Section II-G, namely the assumptions on the vessel's acceleration.

B. Case 2: Position reference fault

In the second case, a position reference system was set to drift at a rate of 0.4 m/s up to a maximum fault of 20 meters. The fault was introduced at $t = 1000$ seconds. The vessel was keeping its position at the origin. The simulation results are shown in Figs. 9 and 10. The performance of the translational motion observer when it comes to estimating the position accurately is less than optimal, but our objective with this observer is solely to detect and isolate failures.

To detect the fault is trivial from Fig. 9 and since we have diverging estimates. A vertical dotted line in the figure marks the time when a fault has been the detected by comparing GNSS measurements. From Fig. 10 showing the position measurement errors of the translational motion observer, it is possible to isolate the faulty output from GNSS 1. A

TABLE I
Measurement noises

Measurement	Std. dev.	Markov time constant
IMU acceleration	0.002 m/s^2	-
IMU gyro	0.08 deg/s	-
Position reference system x and y	1.1 m	4 min
Position reference system z	2.2 m	4 min
Gyrocompass	0.07 deg	-

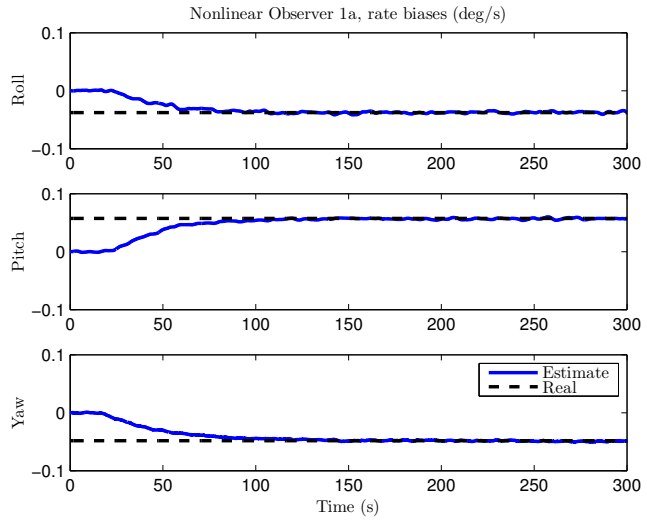

Fig. 3. Case 1: Nonlinear Observer 1a IMU gyro bias estimates

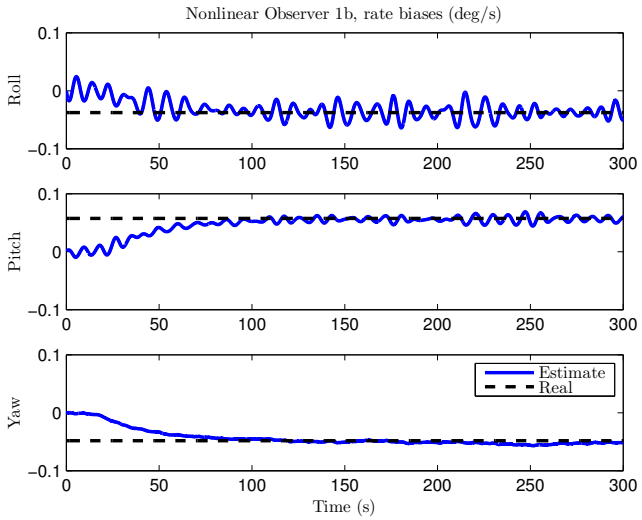

Fig. 5. Case 1: Nonlinear Observer 1b IMU gyro bias estimates.

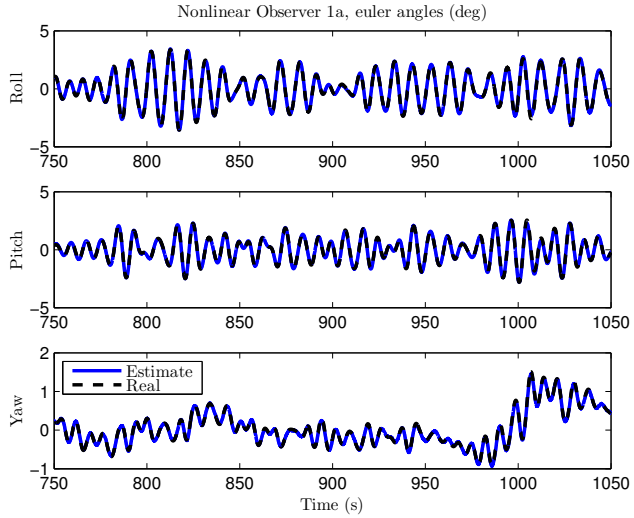

Fig. 4. Case 1: Nonlinear Observer 1a attitude estimates

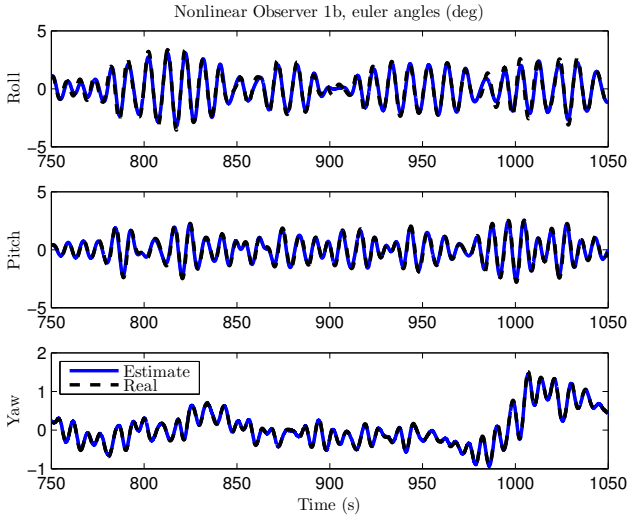

Fig. 6. Case 1: Nonlinear Observer 1b attitude estimates.

significant transient occurs for Observer 1b and 2 during the sensor drift-away. Translational Motion Observer 1a seems to cancel out the position error and keep it at lower level. This is likely due to the fact that it receives its attitude from Nonlinear Observer 1a, which we recall has the GNSS signal as part of the observer equations. When the attitude is estimated with the help of the faulty GNSS signal, the attitude estimate cannot be trusted for use in FDI of that same GNSS signal. However, the output of Observer 1a displays some smaller transients at $t = 1000$ when the position measurement drift starts and at $t = 1050$ when the drifting ends.

C. Case 3: Gyrocompass fault

In the third case, a gyrocompass was set to drift at a rate of 0.4 deg/s up to a maximum fault of 20 degrees. The fault was introduced at $t = 1000$ seconds. The vessel was as before keeping its position at the origin. The results can be seen in Figs. 11 and 12. As for the posref fault case, detecting a fault is trivial from looking at the estimates themselves (Fig. 11 as they diverge. By considering the heading estimation error (Fig. 12), we see that we may in this case use any of the observers to isolate the fault with the chosen thresholds.

D. Discussion

As the simulation results demonstrate, Nonlinear Observer 1a seems to have a slight edge on the others when it comes to fault free attitude estimation. This is most likely due to the fact that Nonlinear Observer 1a estimates the acceleration in the n-frame, while the others assumes that the acceleration is negligible. In our simulations, wave excitations impose motion on the vessel, especially in the heave direction, which will make significant contributions to the accelerometer measurement $\boldsymbol{a}^b_{IMU}$.

Nevertheless, all observers were able to isolate a faulty

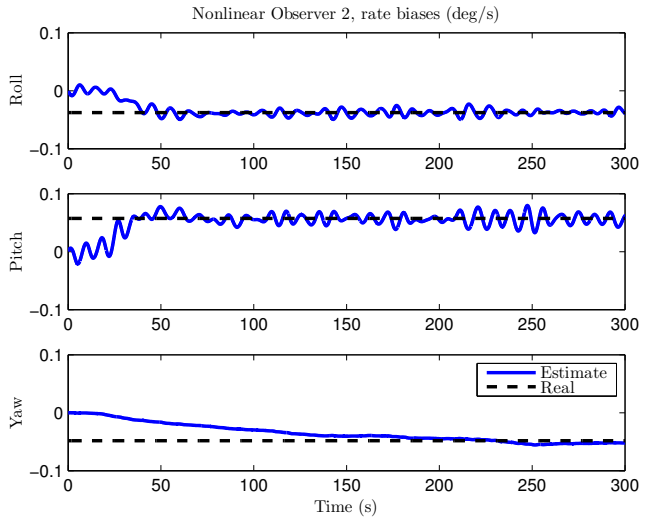

Fig. 7. Case 1: Nonlinear Observer 2 IMU gyro bias estimates.

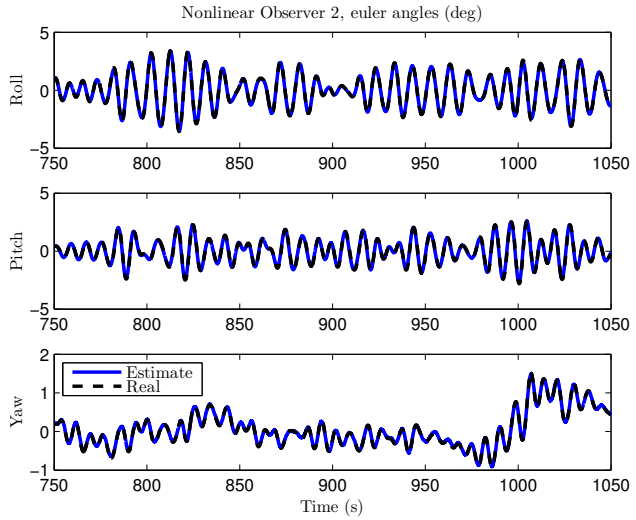

Fig. 8. Case 1: Nonlinear Observer 2 attitude estimates.

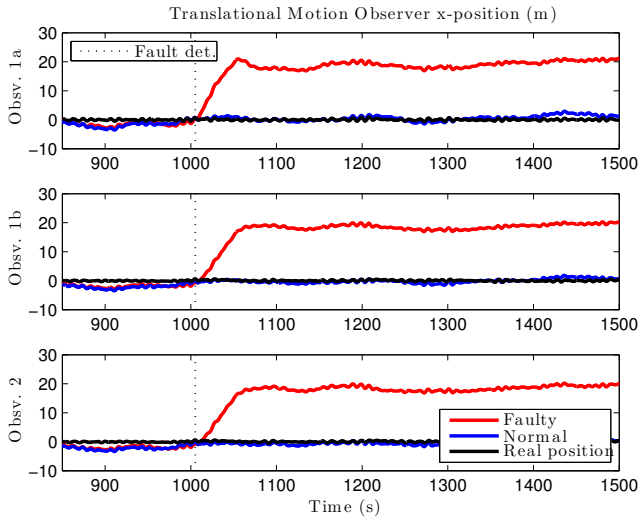

Fig. 9. Case 2: Translational Motion Observer position estimates and true position during posref fault test.

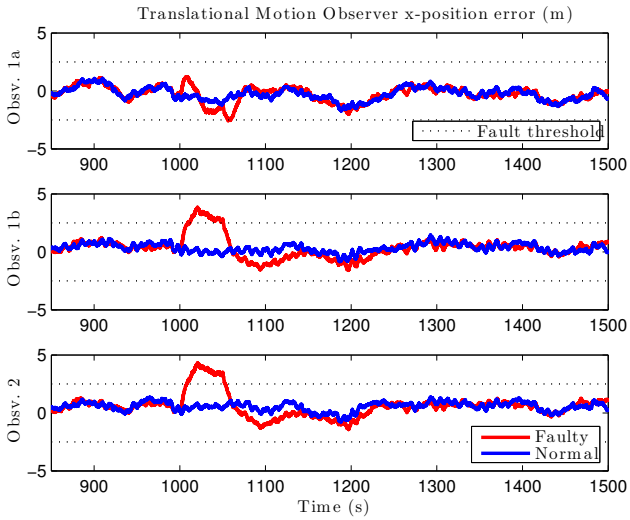

Fig. 10. Case 2: Translational Motion Observer position errors during posref fault test, where the error is the difference between the measurement and estimate.

gyrocompass, and by using the attitude from the Nonlinear Observers 1b and 2 as input to a Translational Motion Observer aided by GNSS, we were able to detect and isolate a drift in GNSS measurement. By doing some appropriate tuning, Nonlinear Observer 1a in the same cascade may be able to isolate the fault as well. However, that could impair the observer's performance and stability. In [21], there are methods that describe applying a filter to the measurement error, in order to generate *residuals*. These filters should be designed so that noise and other error sources are masked out from the residual. Applying such a filter to the topmost output shown in Fig. 10, may yield good fault isolation results while keeping up performance.

In [12] results very similar to Figs. 9 - 12 were obtained. However, in this current paper some of the restrictive assumptions in the previous work have been removed, due to the nonlinear observers that we employ. First, we now estimate roll and pitch alongside with yaw, instead of considering the two former as known external signals. Second, in [12] the IMU gyro bias was assumed to be accounted for beforehand, and was out of scope of the paper. The observers we use in this paper estimate the gyro bias, while still being able to perform the FDI tasks completed in [12].

IV. Conclusion

In this paper we have compared three nonlinear attitude observers, in an attitude and bias estimation test, and in two FDI scenarios. Nonlinear Observer 1a was found to be slightly more suitable than Nonlinear Observer 1b and 2 when it came to fault free attitude and bias estimation. In the first FDI test case, the nonlinear observers were paired with a translational motion observer aided by GNSS to detect and isolate a position fault. Nonlinear Observer 1b and 2

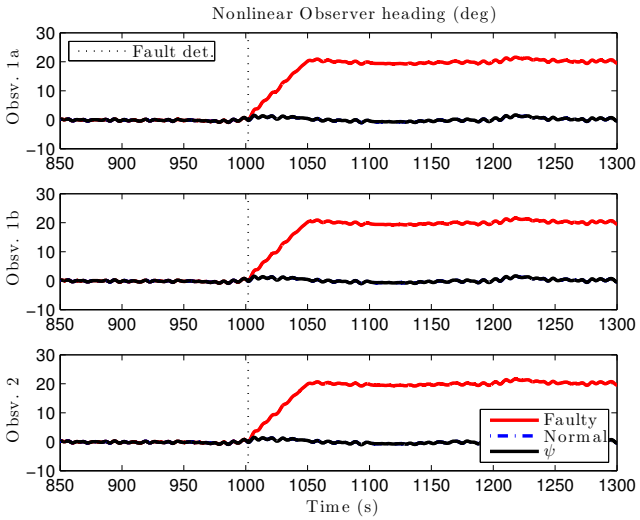

Fig. 11. Case 3: Nonlinear Observer heading estimates and true heading during gyrocompass fault test.

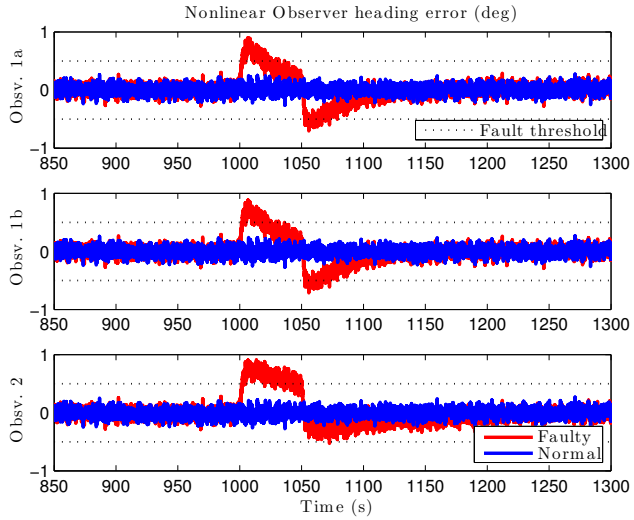

Fig. 12. Case 3: Nonlinear Observer heading error during gyrocompass fault test, where the error is the difference between the measurement and estimate.

performed well in this case, but Nonlinear Observer 1a fell a bit short. In the second FDI case, the attitude observers were used to detect and isolate a gyrocompass fault. In this case, all three observers managed to isolate the source of the fault.

Acknowledgment

The author would like to thank Torleiv Håland Bryne at the Department of Engineering Cybernetics, NTNU for providing fruitful discussions and valuable input.

References

[1] *Guidelines for Vessels with Dynamic Positioning Systems. Maritime Safety Committee, Circular 645*, International Maritime Organization, June 1994.

[2] *Rules for Classification of Ships, Part 6 Chapter 7. Dynamic Positioning Systems*, Det Norske Veritas, July 2013.

[3] *Guide for Dynamic Positioning Systems*, American Bureau of Shipping, November 2013.

[4] H. Chen and T. Moan, "DP incidents on mobile offshore drilling units on the Norwegian Continental Shelf," in *Advances in Safety and Reliability - Proceedings of the European Safety and Reliability Conference, ESREL 2005*, vol. 1, 2005, pp. 337–344.

[5] H. Chen, T. Moan, and H. Verhoeven, "Safety of dynamic positioning operations on mobile offshore drilling units," *Reliability Engineering & System Safety*, vol. 93, no. 7, pp. 1072 – 1090, 2008.

[6] Y. Paturel, "PHINS - an all-in-one sensor for DP applications," in *MTS Dynamic Positioning Conference, 28-30 September 2004, Houston, TX*, 2004.

[7] M. Berntsen and A. Olsen, "Hydroacoustic aided inertial navigation system - HAIN a new reference for DP," in *Dynamic Positioning Conference, October 9-10*, 2007.

[8] B. Vik and T. Fossen, "A nonlinear observer for GPS and INS integration," in *Proceedings of the 40th IEEE Conference on Decision and Control*, vol. 3, Piscataway, NJ, USA, 2001, pp. 2956 – 61.

[9] D. Russell, "Integrating INS and GNSS sensors to provide reliable surface positioning," in *Dynamic Positioning Conference October 9-10*, 2012.

[10] R. Stephens, F. Crétollier, P.-Y. Morvan, and A. Chamberlain, "Integration of an inertial navigation system and DP," in *Dynamic Positioning Conference October 7 - 8*, 2008.

[11] M. Blanke, "Diagnosis and fault-tolerant control for ship station keeping," in *Intelligent Control, 2005. Proceedings of the 2005 IEEE International Symposium on, Mediterrean Conference on Control and Automation*. IEEE, 2005, pp. 1379–1384.

[12] R. H. Rogne, T. A. Johansen, and T. I. Fossen, "Observer and IMU-based detection and isolation of faults in position reference systems and gyrocompass with dual redundancy in dynamic positioning," in *2014 IEEE Multi-Conference on Systems and Control*, 2014, pp. 83 – 88.

[13] S. Salcudean, "A globally convergent angular velocity observer for rigid body motion," *IEEE Transactions on Automatic Control*, vol. 36, no. 12, pp. 1493 – 7, 1991.

[14] R. Mahony, T. Hamel, and J.-M. Pflimlin, "Nonlinear complementary filters on the special orthogonal group," *IEEE Transactions on Automatic Control*, vol. 53, no. 5, pp. 1203 – 1218, 2008.

[15] H. F. Grip, T. I. Fossen, T. A. Johansen, and A. Saberi, "Attitude estimation using biased gyro and vector measurements with time-varying reference vectors," *Automatic Control, IEEE Transactions on*, vol. 57, no. 5, pp. 1332–1338, 2012.

[16] ——, "Nonlinear observer for GNSS-aided inertial navigation with quaternion-based attitude estimation," in *Proceedings of the American Control Conference*, Washington, DC, United states, 2013, pp. 272 – 279.

[17] M.-D. Hua, G. Ducard, T. Hamel, R. Mahony, and K. Rudin, "Implementation of a nonlinear attitude estimator for aerial robotic vehicles," *IEEE Transactions on Control Systems Technology*, vol. 22, no. 1, pp. 201 – 13, 2014.

[18] T. I. Fossen, *Handbook of marine craft hydrodynamics and motion control*. John Wiley & Sons, 2011.

[19] A. Loría and E. Panteley, "2 cascaded nonlinear time-varying systems: Analysis and design," in *Advanced topics in control systems theory*. Springer, 2005, pp. 23–64.

[20] P. Martin and E. Salaün, "Design and implementation of a low-cost observer-based attitude and heading reference system," *Control Engineering Practice*, vol. 18, no. 7, pp. 712–722, 2010.

[21] M. Blanke, "Enhanced maritime safety through diagnosis and fault tolerant control," in *Control Applications in Marine Systems 2001 (CAMS 2001) Proceedings volume from the IFAC Conference*, Kidlington, UK, 2001, pp. 1 – 19.

[22] M. Blanke, M. Kinnaert, J. Lunze, and M. Staroswiecki, *Diagnosis and Fault-Tolerant Control*, 2nd ed. Springer-Verlag Berlin Heidelberg, 2006.

[23] F. Gustafsson, "Statistical signal processing approaches to fault detection," *Annual Reviews in Control*, vol. 31, no. 1, pp. 41 – 54, 2007.

[24] "MSS. Marine Systems Simulator," Viewed 01.05.2014, www.marinecontrol.org,, 2010.